RESEARCH REPORT

VTT-R-00725-24

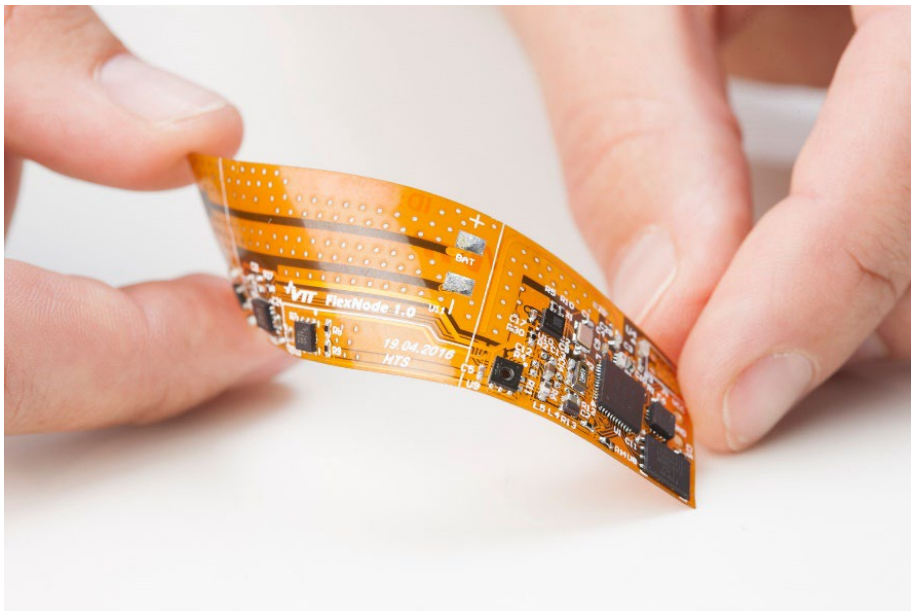

SAFER-FN-CAMP: Assessment of alkali-silica reaction and aggressive aqueous attack in concrete 2024

Authors: Yushan GU

Confidentiality: VTT Public

Version: 21.01.2025

VTT

beyond the obvious

Report's title

VTT internal reports-SAFER-FN-CAMP: Assessment of alkali-silica reaction (ASR) and aggressive aqueous attack (AAA) in concrete 2024

Customer, contact person, address	**Order reference**
National Nuclear Safety and Waste Management Research Program SAFER2028	-
Project name	**Project number/Short name**
Finnish Nuclear Concrete Ageing Management Project, WP 2 Alkali silica reaction (ASR) and aggressive aqueous attack (AAA) on structural performance	137831/FN-CAMP
Author(s)	**Pages**
Yushan GU	20
Keywords	**Report identification code**
Alkali-silica reaction; Aggressive aqueous attack; durability of concrete; modelling	VTT-R-00725-24

Summary

This report summarises the study conducted in the SAFER2028 FN-CAMP project in 2024. The main objective of the WP2 of the FN-CAMP project is to assess the deterioration mechanism induced by alkali-silica reaction (ASR) and aggressive aqueous attack (AAA) on concrete structures in nuclear power plants (NPPs). To achieve this goal, assessment tools to predict the ASR expansion of concrete and evaluate the deterioration of concrete exposed to an aggressive aqueous environment are developed within the project. In the first part, the ASR assessment tool is explored in sensitivity analysis cases, assessing the impact of temperature and relative humidity on ASR expansion. Low temperature and relative humidity are found efficient methods to prevent ASR in concrete. In the second part, the durability performance of cementitious materials exposed to Na_2SO_4 /and NaOH solutions is predicted, and the impact of porosity on the durability performance of cementitious materials exposed to sulfate solutions is assessed. The results concluded that high pH in exposure solutions and low porosity of cementitious materials can significantly improve the durability performance of materials.

Confidentiality	VTT Public

Espoo 24.1.2025

Written by	**Reviewed by**
Yushan GU Research scientist	Pirkko Kekäläinen Research Scientist

VTT's contact address

VTT Technical Research Centre of Finland Ltd, P.O. Box 1000 (Kemistintie 3, Espoo), FI-02044 VTT, Finland

Distribution (customer and VTT)

SG3 of SAFER28

Approval

VTT TECHNICAL RESEARCH CENTRE OF FINLAND LTD

Date:	17.3.2025
Signature:	DocuSigned by: Miguel Ferreira DA102FF7B375410...
Name:	Miguel Ferreira
Title:	Research Team Leader

Contents

1. Introduction

The SAFER2028 Finnish Nuclear Concrete Ageing Management project (FN-CAMP) aims to assess the safety performance of Finnish nuclear power plants (NPPs) and radioactive waste repository concrete structures. The outcomes support their ageing-related aspects based on the needs of Finnish End Users. This report summarises the study conducted in WP2 Alkali silica reaction (ASR) and aggressive aqueous attack (AAA) on the structural performance of the SAFER2028 FN-CAMP project for 2024. Using the assessment tool developed in 2023 [1], several improvements are made, and sensitivity analyses are conducted. The main objective of WP2 in 2024 is to assess the deterioration mechanism induced by alkali-silica reaction (ASR) and evaluate the impact of temperature and relative humidity (RH) on ASR expansion. In addition, WP2 also aims to assess the durability performance of cementitious materials exposed to Na_2SO_4 and Na_2SO_4 + NaOH solutions, one of the considered aggressive aqueous attack (AAA) conditions.

2. WP2 Alkali-silica reaction (ASR) and aggressive aqueous attack (AAA) on structural performance

2.1 T2.1 ASR on structural performance

This task aims to develop an assessment tool to evaluate the deterioration of concrete subject to ASR. A thermo-chemo-cracking model [2] is adopted to simulate the ASR expansion, with some parameters characterising the property of the material. The basic model calculating the incremental volumetric ASR strain was established in 2023, and it replicated the expansion curves of concrete subject to ASR. The model softly couples the kinetics of chemical reactions and mechanics of cracking that affect volume expansion and the degradation of mechanical properties. To be more specific, it considers the impact of tensile cracking, compressive stresses, temperature, and RH based on empirical equations. Work in 2024 focuses on analysing the effects of temperature and RH on ASR expansion and exploring the capabilities and limitations of our tool. Before presenting the results and findings in 2024, it is worth recalling the ASR model established in 2023 [1]. The main input data to the model include:

- Material properties regarding mechanics (e.g., Young's modulus, compressive and tensile strengths, factors representing the residual when the material is under tension and tensile, etc.);
- Environmental exposure conditions (e.g., temperatures, relative humidity);
- ASR expansion data (i.e., final expansion magnitude ε^{∞}, initial values of $\tau_C(\theta_0)$, $\tau_L(\theta_0)$).

$\tau_L(\theta_0)$ is the latency time at the reference temperature θ_0, corresponding to the inflexion point in the expansion curve, see Figure 1. $\tau_C(\theta_0)$ is the characteristic time at the reference temperature, defined as the intersection of the tangent at τ_L with the asymptotic unit value of ξ. The simulation process starts by demanding ε^{∞} and initial values of $\tau_C(\theta_0)$ and $\tau_L(\theta_0)$ to the model as input. The model then adjusts the values of τ_C and τ_L by comparing the predicted expansion to the experimental data, and stops until their difference reaches a target criterion.

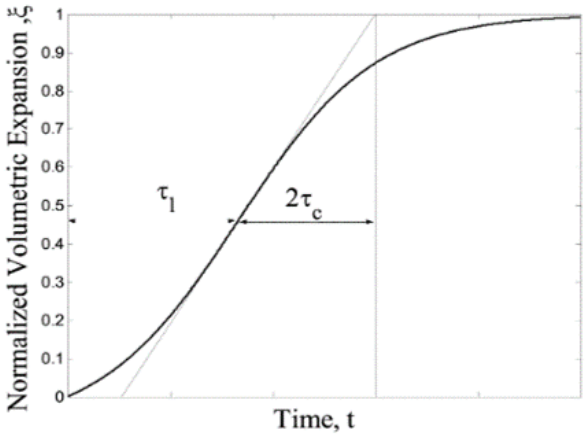

Figure 1: Normalised expansion curve ($\xi(t) = \varepsilon_{F,Vol}^{AAR}(t)/\varepsilon_{AAR}^{\infty}$).

2.1.1 Literature review

Three key parameters influencing the rate and extent of ASR are alkali content, temperature, and RH [3], [4]. Among them, temperature has a dominant role in influencing the kinetics of ASR. It may take several years for ASR to manifest and several decades for a stabilised swelling. The impact of temperature on ASR expansion has been generally accepted by researchers, i.e. a higher temperature leads to faster expansion kinetics [5]. However, different opinions have been brought up regarding the impact of temperature on final expansion. A limited impact was believed in [6], while a greater expansion was observed at relatively lower temperatures in [7], [8]. This could be explained by the pessimum effect of temperature on the final expansion as pointed out in [8], [9], [10]. The pessimum temperature was reported as approximately 40 ℃ [9], [11]. However, the mechanism behind this is not clear yet, and it may depend on the type of reactive aggregates and other environmental factors.

Moisture content of concrete, i.e., RH, plays another key role in the initiation and progress of the reaction. A threshold of 80% has been referenced as a necessity to initiate the reaction, which might depend on other factors like temperature, alkali content, aggregate type, etc [12]. To highlight the role of temperature influencing the RH threshold for the initiation of ASR, thresholds were reported as 80% at 23 ℃ and 75% at 38 ℃ [13]; 80-85% at 20 ℃ [14]; 75% at 40 ℃ [15]. Generally, concrete stored in a higher RH condition experienced a higher expansion [6]. An increased RH will alter the dissolution of remaining silica, the reaction of the products, and the swelling of the gel leading to larger expansions. However, at high RH, particularly stored in solutions, concrete specimens could be prone to alkali leaching [16].

2.1.2 Sensitivity analyses of temperature

The role of temperature in ASR expansion is included in the assessment tool as the function $\xi(t,\theta)$, representing a normalised expansion degree to the final expansion. It is well illustrated in Eq. (1) and Figure 1. For a better understanding, the definition of Eq. (1) is recalled as follows:

$$\xi(t,\theta) = \frac{1 - e^{-\frac{t}{\tau_C(\theta)}}}{1 + e^{-\frac{t-\tau_L(\theta,I_\sigma,f_c')}{\tau_C(\theta)}}} \qquad (1)$$

The function $\xi(t,\theta)$, a thermodynamically based model, was proposed by [6] based on experimental tests of 600 specimens with various mixtures, and ambient & mechanical conditions. The model replicates the

expansion evolution as a time and exposure temperature function. More sophisticated definitions of the coefficients $\tau_C(\theta)$ and $\tau_L(\theta, I_\sigma, f_c')$ were proposed in [17] showing the thermal dependency as:

$$\tau_C(\theta) = \tau_C(\theta_0)\, exp[U_C(\frac{1}{\theta} - \frac{1}{\theta_0})] \quad (2)$$

$$\tau_L(\theta, I_\sigma, f_c') = f(I_\sigma, f_c')\, \tau_L(\theta_0) exp[U_L(\frac{1}{\theta} - \frac{1}{\theta_0})] \quad (3)$$

where U_L and U_C are the activation energies minimum energy required to trigger the reaction for the latency and characteristic times. Examples regarding the values of $U_L = 9400 \pm 500\, K$ and $U_C = 5400 \pm 500\, K$ were mentioned in [17], which were based on Larive's experimental data reported in [6].

To better understand the impact of temperature on ASR expansion, four different values, i.e., 7 ℃, 15 ℃, 25 ℃, and 38 ℃ are considered for sensitivity analyses. Figure 2 compares the predicted ASR expansion in concrete when exposed to various temperatures, where the same input ($\tau_C(\theta_0)$, $\tau_L(\theta_0)$, and ε^∞) was used and the calculation was implemented in one iteration. It is observed that a higher temperature leads to faster incremental kinetics. For example, ASR expansion is stabilised at around 100 days when it is stored at 25 ℃, while the duration is almost double at 15 ℃ and tripled at 7 ℃. The impact has inspired the idea of employing a relatively higher temperature, such as 38 ℃, for accelerating ASR in laboratory tests [18]. An impact of temperature on the final expansion is also observed: a higher temperature tends to lead to a higher final expansion magnitude, and the increasing impact is even highlighted at a higher temperature. For example, the final expansion increases 2.5% from 15 ℃ to 25 ℃, and the increment is approximately 6% when the temperature increases from 25 ℃ to 38 ℃. However, this observation is contrary to the findings reported in the literature, where a limited impact of temperature on final expansion was observed or a higher temperature leads to a relatively lower final expansion, as explained in the section 2.1.1. The reason for the discrepancy in our model is that final expansion is calculated using incremental deformation as a function of time, where faster incremental kinetics at higher temperatures are taken into account. It can be concluded that predicting the ASR expansion under various temperatures based on one experimental curve at a certain temperature is not properly addressed in the current model. Moreover, the different opinions regarding the impact of temperature on final expansion bring challenges to the simulation work. Therefore, using the expression of normalised expansion is recommended when studying the impact of temperatures.

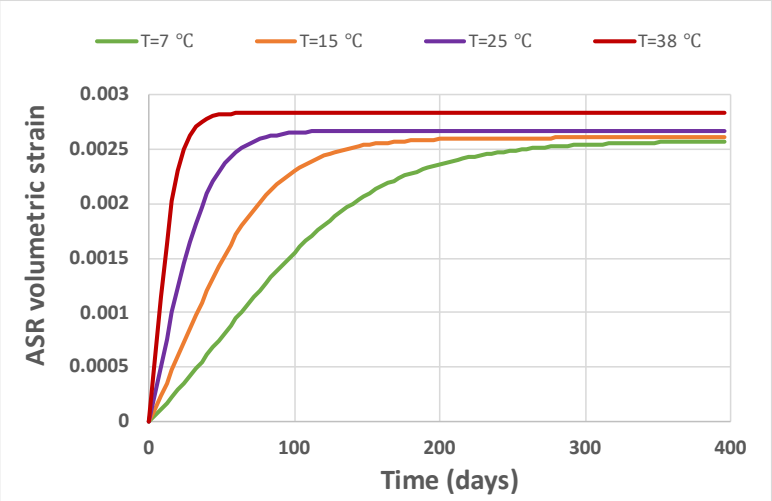

Figure 2: Predicted ASR volumetric strain in concrete with temperatures ranging from 7 ℃, 15 ℃, 25 ℃, and 38 ℃.

2.1.3 Sensitivity analyses of RH

In [2], the impact of RH on ASR expansion is considered as a reduction function $f(h)$, thus $0 < f(h) \leq 1$. It is formulated as:

$$f(h) = h^m \tag{4}$$

where *h* is the RH, and *m* is the influencing factor. For a concrete structure constantly immersed under water, e.g., dams, we can reasonably assume $f(h) = 1$ for all exposure conditions. However, for the structures not fully saturated with moisture, e.g., bridges, and some parts of NPPs, the impact of various RH on ASR needs to be addressed. Eq. *(4)* was first proposed in [19] according to a curve published in [20], showing the evolution of ASR expansion referring to free expansion ε_{100} at RH=100% vs. RH, see Figure 3 and Eq. *(5*). It describes well that ASR is only triggered when RH is above a certain value, e.g., 70%. Under the value, there is not enough moisture for reaction initiations. Above the threshold, a higher RH leads to a higher expansion, and significant expansions occur for RH greater than approximately 85%.

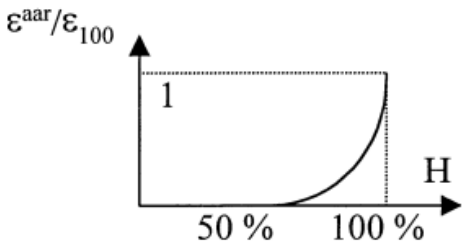

Figure 3: A simplified power function showing the evolution of ASR expansion as a function of RH [19].

$$\varepsilon^{ASR}/\varepsilon_{100} = h^m \text{ (m=8)} \tag{5}$$

Figure 4 shows the predicted ASR volumetric strains in concrete with various RHs, including 50%, 70%, 90%, and 100%, where identical input ($\tau_C(\theta_0)$, $\tau_L(\theta_0)$, and ε^{∞}) was considered and the calculation was completed in one iteration. No obvious expansion is observed when RH is 50%, and slight expansion is observed when RH increases to 70%. Significant increases in expansion occur when RH reaches above 90%, highlighting the important role of water triggering ASR expansion in concrete. It also indicates low RH as a method to mitigate ASR. Similar findings have been reported in the literature. Among them, [21] showed length variations of concrete specimens prepared with reactive aggregates under various temperatures (21, 38, and 60 ℃) and RHs (100%, 90%, 82%, 75%, and 62%) for 1 year, see Figure 5. Discard the weird point measured at 100% RH and 68 ℃, which was explained as probably due to alkali-leaching, a higher RH tends to lead to a higher expansion magnitude. The data was then converted following the expression of Eq. *(5*), and the curve was fit with power functions as shown in Figure 6. The parameter *m* was calibrated as a value of around 2.2, which is different to the value reported in [19]. It means that the parameter is material-dependent and requires calibration for different concrete mixes. With this relationship between RH and expansion, we can predict the ASR expansion of concrete under various RHs based on one set of experimental data at a certain RH condition.

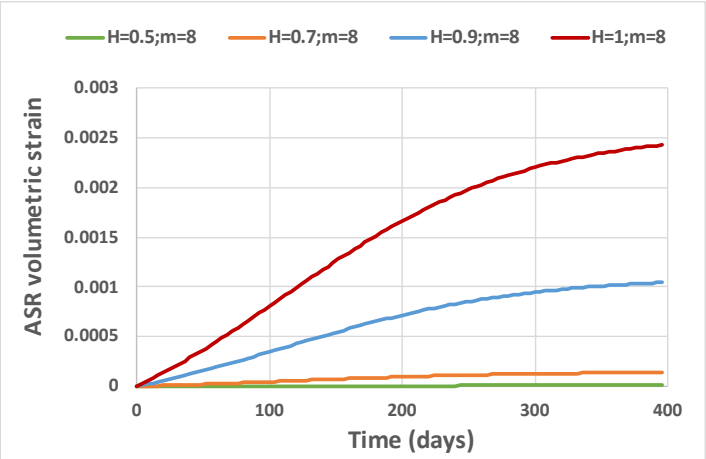

Figure 4: Predicted ASR volumetric strains in concrete with various RHs: 50%, 70%, 90%, and 100%.

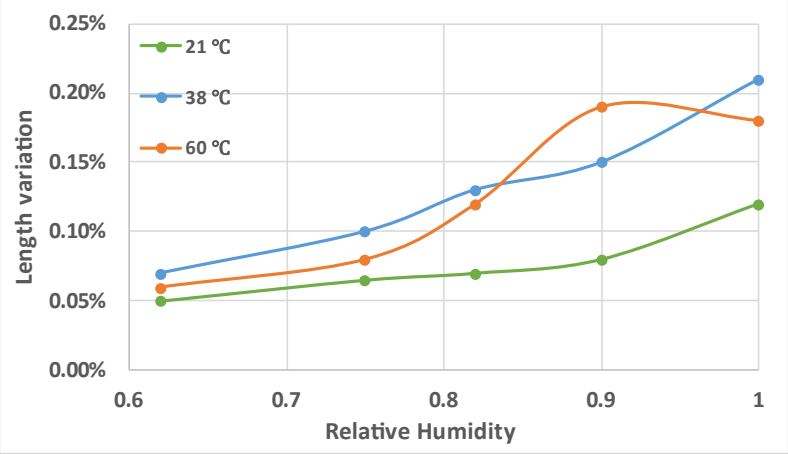

Figure 5: Length variations of concrete samples exposed to various temperatures and RHs collected from [21].

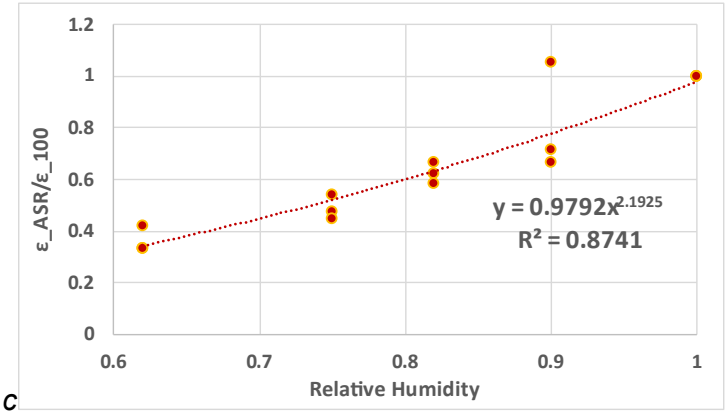

c

Figure 6: Calibrated power function following the Eq. (5) based on the data collected from [21].

2.2 T2.2 AAA on structural performance

An assessment tool based on reactive-transport modelling is developed in this task to evaluate the deterioration of concrete exposed to an aggressive environment, which includes pure water, sodium sulfate solution, groundwater, and seawater. This order is determined according to the number of reactions that may occur between the material and the exposed solution. In 2023 the performance of concrete exposed to leaching was simulated. The main degradation phenomenon observed was portlandite (CH) dissolution, calcium silicate hydrate (C-S-H) decalcification, and calcite precipitation. In 2024 the performance of concrete exposed to Na_2SO_4 solution is evaluated, and the profiles/evolution of the mineralogical phases and porosity are simulated. The results contribute to determining the degradation depth of concrete due to external sulfate attack, and the deterioration rate at different exposure durations, which will provide an assessment tool for the existing structures for extended service life.

Sulfate attack is considered one of the main problems affecting the durability of cement-based materials, which is a problem perplexing engineers and researchers. It has been a concern of concrete technologies since the early years of the 19th century, and thus the subject of sulfate attacks has been studied extensively. Sulfate ions, commonly present in sulfate-containing environments (marine environment or groundwater) or construction materials, are unavoidable in engineering fields. Sulfate attacks in concrete encompass a series of chemical and physical interactions that occur between hardened cement pastes and sulfates, which result from the chemical reactions between the tricalcium aluminate (C_3A) contained in Portland cement and sulfate ions supplied by different sources, e.g. cement materials in the case of internal sulfate attack (ISA) and exposure solution in the case of external sulfate attack (ESA). The latter is the case we will focus on in this work.

Cements undergo deterioration in sulfate-rich environments, such as groundwater, rivers, seawater, and sewage, and loss of strength in concrete structures is foreseen [22], [23], [24], [25]. The damage depends on the chemical interaction between the aggressive environment and the cement-based materials. The deterioration relates to the dissolution of CH and the sophisticated decalcification of C-S-H [26]. It results in changes in the microstructure, loss of strength, propagation of microcracks, softening, decohesion, expansion or even spalling [27]. The loss of mechanical performance has been attributed to the formation of secondary sulfate-bearing phases, e.g., expansive compounds like ettringite [28]. Some other theories attribute the damage to the formation of gypsum [29], while extensive gypsum precipitation is believed to form after the occurrence of cracks without contributing to the macroscopic expansion [30], [31], [32].

2.2.1 Assessment tool

The reactive-transport modelling tool HP1, which couples Hydrus-1D with PHREEQC geochemical code, is used to predict the evolution and profile of mineralogical phases and pore water composition in the cementitious system. The simplified cement system, geometry, and input data are presented in this subsection.

2.2.1.1 Simplified cement model

The chemical processes involved are assumed to evolve under thermodynamic equilibrium, including the reactions between each cementitious material. A thermodynamic database, CEMDATA v18 [33] (https://www.empa.ch/cemdata) – PHREEQC version is used to represent the cement system, where a comprehensive selection of cement hydrates on ordinary Portland cement and alkali-activated materials is available. Moreover, the equilibrium constants (i.e., log K values) for each equilibrium reaction under various conditions, standard molar volumes for each mineral, etc., are available in this thermodynamic database. The calcium silica hydrate is considered the ideal solid solution with six end members (CSHQ-JenD, CSHQ-JenH, CSHQ-TobD, CSHQ-TobH, KSiOH, and NaSiOH), following the CSHQ model proposed in [34]. All cementitious materials are considered fully equilibrated as initial conditions in the reactive transport simulations. The cement hydration calculations have been carried out using the Gibbs

energy minimization approach (with the GEM-Selektor software [35]). It is worth noting that aggregates are considered chemically inert in the reactive transport model in this work.

The chemical reactions lead to porosity changes in cementitious materials due to the dissolution/ precipitation of phases, which changes the permeability property of the cementitious barrier. Therefore, the porosity and permeability feedback are considered important factors when simulating the chemical evolution in a massive concrete structure. In the case of considering the feedback, the porosity is updated in each time step of the chemical calculations by adding the precipitated phases and removing the dissolved ones in volume fractions. The resulting change of porosity is then transferred to the transport equations as feedback and the corresponding diffusive properties are updated.

2.2.1.2 Simplified geometry

The reactive transport model considers the cementitious system in an initially fully saturated state, and the material has been conceptualised as homogeneous porous media. The schematic layout of the system is presented in Figure 7. The total length of the considered cementitious system is 1 m, and it is divided into 10 elements with Δx=0.1 m. Boundary conditions (BD) are imposed on two sides of the system. The initial composition of the exposed solution, initial phases, and initial composition of pore solution in the mortar will be defined in the section 2.2.1.3.

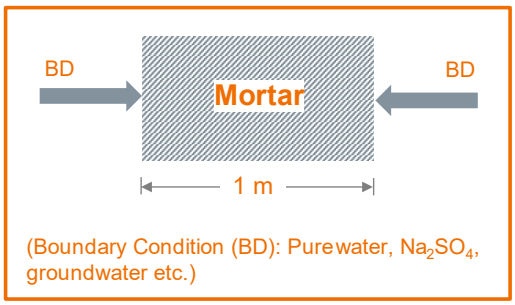

Figure 7: Schematic layout of the simulated cementitious system and the surrounding boundary conditions.

2.2.1.3 Input data

Cementitious materials are considered fully equilibrated as initial conditions in the reactive transport simulations. The fully hydrated mortar/concrete includes portlandite, CSHQ, and calcite as the main minerals, and the C-S-H solid solution shows a relatively higher amount of the JenD (Ca/Si=2.25) and TobD (Ca/Si=1.25) end members. The equilibrated pore water in mortar shows a highly alkaline pH due to the high concentrations of Na and K. The calculated porosity of the mortar is 29% based on the cement hydration calculations. A pore diffusion coefficient of 1.0E-9 m^2/s is selected, which considers the high interconnection of the pore structure in the mortar and a corresponding high impact on transport property. Table 1 summarizes the initial mineral phases present in the cementitious materials, and Table 2 shows the composition of the initial pore solution of concrete.

Table 1: Initial mineral phases in cementitious materials [36].

Mineral [mol/kg water]	Mortar
CSHQ-JenD	1.5092
CSHQ-JenH	0.9835
CSHQ-TobD	1.1345

Table 2: Composition of the pore solution in cementitious materials [36].

Species [mol/L]	Mortar
pH	13.09
pe	-6.8
Ca	2.65e-3

CSHQ-TobH	0.0486
KSiOH	0.1340
NaSiOH	0.0420
Ettringite	0.1207
Monocarbonate	0.2092
Calcite	0.2445
$C_3FS_{0.84}H_{4.32}$	0.1460
Portlandite	3.6971
Hydrotalcite	0.0822

Mg	2.94e-9
Na	9.13e-3
K	1.53e-1
Fe	4.98e-8
Al	3.30e-5
Cl^-	1.95e-7
C(4)	3.33e-5
S(6)	5.54e-4
Si	3.79e-5
Sr	1.00e-10

The concrete interaction with the surrounding environment is simplified to a fixed concentration as a boundary condition, simulating the exposure solutions. In this case, diffusion will be the only process influencing the chemical evolution in the system. Two cases of exposure solutions are considered, (i) Case 1: Na_2SO_4 solution, where the degradation of mortar due to sulfate attack and leaching is foreseen; and (ii) Case 2: Na_2SO_4 and NaOH solution, where the degradation of mortar due to leaching is reduced in a certain degree. Table 3 summarises the composition of exposure solutions in the two investigation cases.

Table 3: Composition of exposure solutions in cases 1 and 2.

Species [mol/L]	Solution in Case 1	Solution in Case 2
pH	7	13
Na^+	0.308	0.308
SO_4^{2-}	0.154	0.154

2.2.2 Simulated mineralogical profiles of the cementitious system

2.2.2.1 Simulations of the system in the initial state

Figure 8 shows the initial state of mineralogical phases in the system, where the inert phase marked in grey and empty space represent aggregates and porosity in mortar. The initial volume fraction of aggregates is around 56% and the initial porosity is 29%. The pH value is shown on the secondary axis on the right, which has a highly alkaline pH above 13 at the initial state.

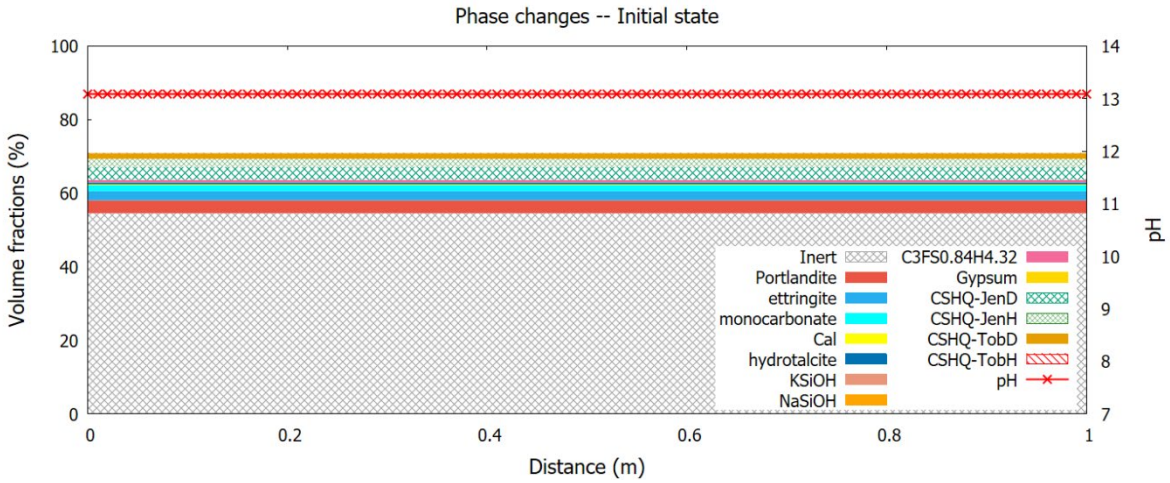

Figure 8: Initial mineralogical phases present in the considered cementitious system.

2.2.2.2 Simulations of the mortar performance exposed to Na_2SO_4 solutions

Figure 9 presents the profile of mineralogical phases in mortar being exposed up to 290 years. The calculation stopped afterwards, as all available mineralogical phases at the border area were consumed. It is shown that after being exposed for 1 year, the degradation of cementitious materials reaches an area 0.05 m away from the boundaries. Two degraded zones are observed. The replacement of monocarbonate by ettringite is observed as the main change between 0.01 and 0.05 m from the boundaries. However, at the very border area, CH and C-S-H are dissolved, and gypsum is precipitated in addition to the formation of ettringite. Since the volume of the dissolved and precipitated phases are comparable, the porosity remains almost constant. Along the exposure, higher amounts of ettringite and gypsum accumulate, and gypsum dissolves when pH decreases below 12.5. Meanwhile, the degradation continues to the inner part of materials. In the simulation after being exposed for 10 years, the degradation reaches around 0.25 m from the boundaries. The main degradation phenomenon focuses on replacing CH and monocarbonate with ettringite, and the formation of ettringite was followed by gypsum.

It can be concluded from the simulation results that the main degradation phenomenon is the dissolution of CH and monocarbonate, decalcification of C-S-H, and the precipitation of ettringite. It has been well known that the degradation of cementitious materials due to sulfate attack is induced by the formation of expansive crystals, i.e., ettringite [28] and gypsum in acid conditions [37], which can be confirmed from the simulations in this study. In addition to sulfate attack, the dissolution of mineralogical phases due to leaching is observed at two boundaries, especially in the last simulation where materials were exposed for 290 years: almost all mineralogical phases are dissolved. The concentration gradient of elements between the pore solution in mortar and the exposure Na_2SO_4 solution leads to the dissolution of phases. To mitigate the leaching process, a mixed solution of Na_2SO_4 and NaOH is considered in case 2.

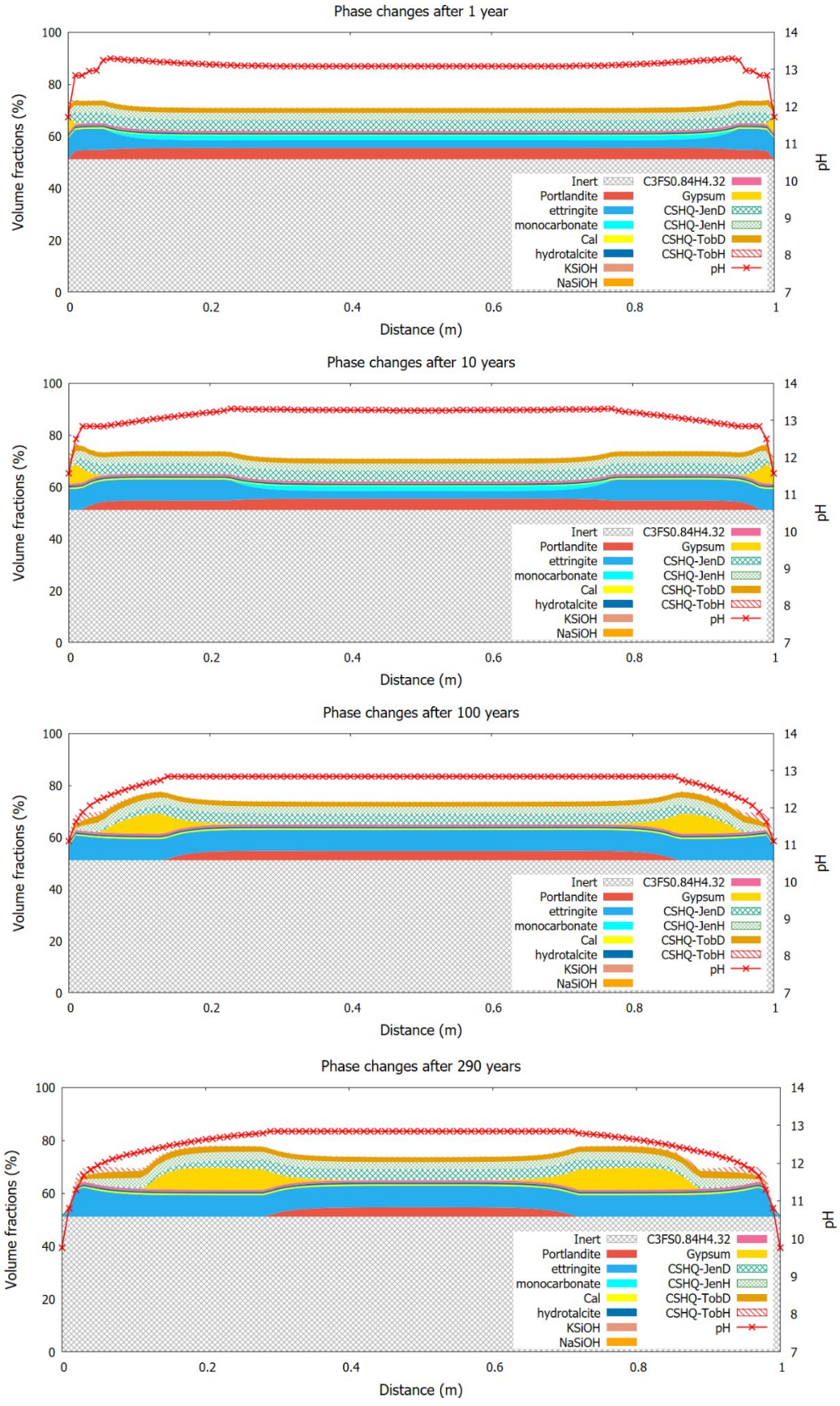

Figure 9: Profiles of the mineralogical phases present in the considered cementitious system exposed to Na_2SO_4 solutions.

2.2.2.3 Simulations of the mortar performance exposed to Na_2SO_4 and NaOH solutions

In case 2, we simulate an exposure solution Na_2SO_4 with a pH of 13 by adding NaOH to prevent the leaching of cementitious materials. Figure 10 shows the simulation results up to 1000 years. It is observed that the main degradation phenomenon is the dissolution of CH and monocarbonate replaced by ettringite, and the pH remains stable at around 13. Compared to case 1, the influenced mineralogical phases are similar, and the transformation of monocarbonate to ettringite is even faster. However, much less CH is dissolved during exposure, which means that the durability performance in cementitious materials is significantly improved. It indicates the importance of a high pH for cement-based materials. The presence of OH^- limits the element concentration gradient between the pore solution in cementitious material and the exposure solution and thus the leaching degree. The formation of gypsum is not observed due to its high solubility at the pH around 13. After being exposed for 1000 years, the dissolution of CH reaches the part 0.25 m from the boundaries, and an obvious increase in porosity is only observed at the very border part.

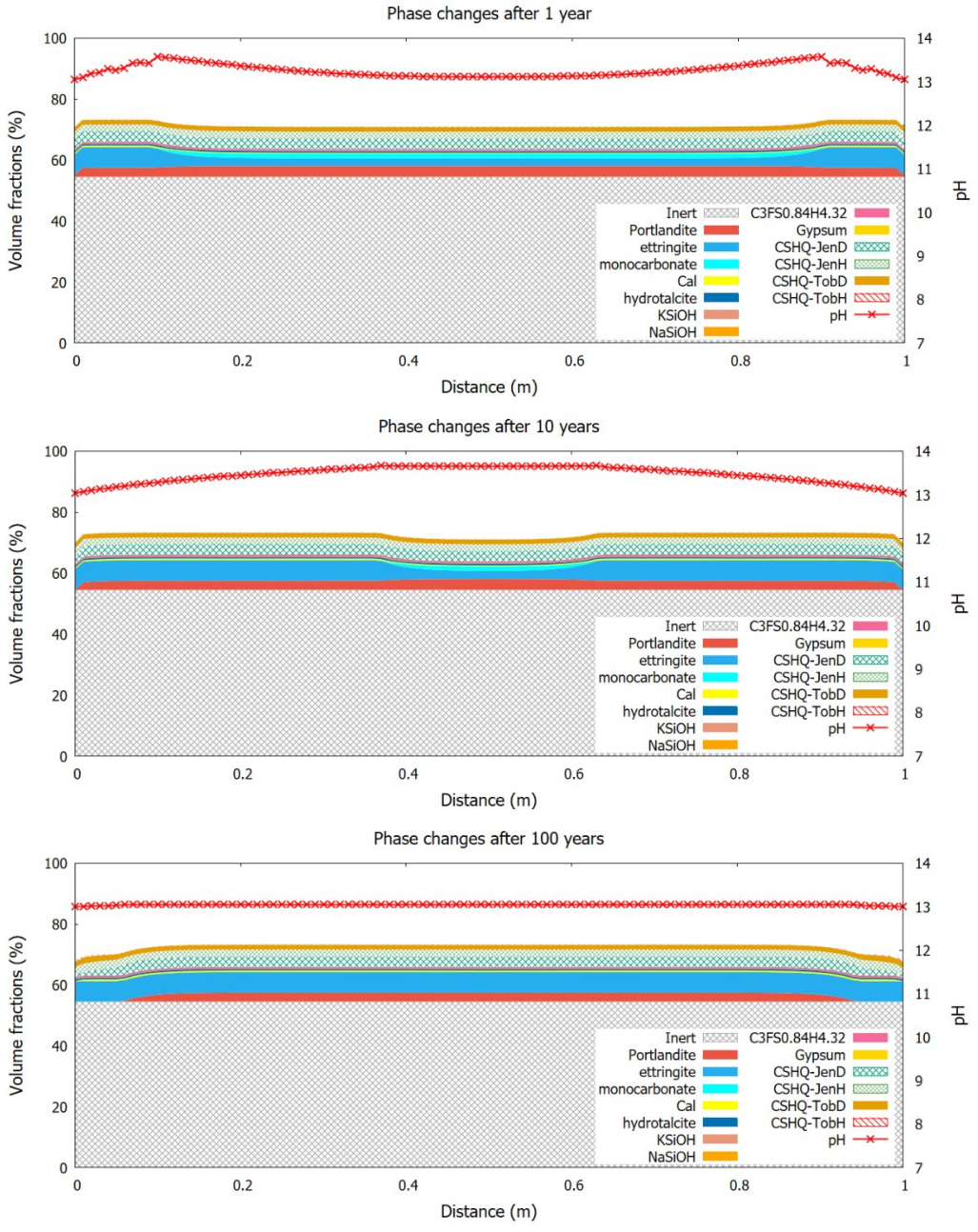

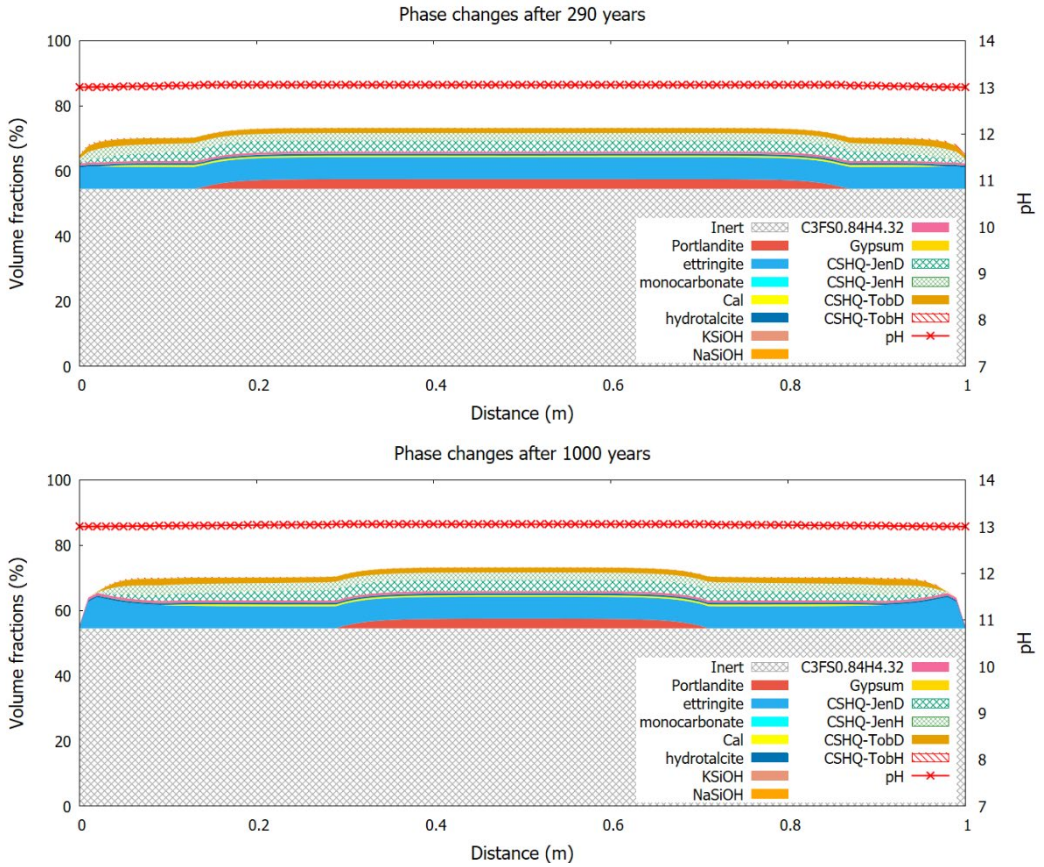

Figure 10: Profiles of the mineralogical phases present in the considered cementitious system exposed to Na_2SO_4 and NaOH solutions.

2.2.2.4 Porosity and permeability sensitivity analyses

Interests regarding the durability performance of slag cement were shown during the SAFER2028 TAG 3.4 1/2024 meeting. Slag, also known as ground granulated blast-furnace slag (GGBS) is commonly used supplementary cementitious material. It has multiple benefits in improving workability and later-age strength, lowering permeability, and reducing carbon footprint [38]. Microstructural characterisation analyses confirmed a densified microstructure and refined pore size distribution in slag cement [39], [40], which can explain its low permeability as reported in [41], [42], [43]. The interest in slag cement motivated us to perform sensitivity analyses regarding porosity and permeability in cementitious materials to assess their durability performances.

In this subsection, mortars with three porosities including 0.25, 0.29, and 0.35 are exposed to Na_2SO_4 solutions, and their behaviour is simulated and compared. Table 4 summarises their service life in years, and it is observed that a higher porosity leads to a shorter service life. This is because a higher porosity accelerates the permeability and transport properties of materials and thus degrades their durability. A more detailed comparison is illustrated in Figure 11, where the profile of mineralogical phases for three mortars after being exposed for 240 years when the service life of the mortar with Φ of 0.35 is almost ended. First of all, the replacement of monocarbonate by ettringite is completed in three cases. The main ongoing degradation phenomena are the dissolution of CH, precipitation of ettringite and gypsum, and leaching at the very border areas. The results indicate the importance of low permeability and porosity for improving long-term durability safety.

Table 4: Comparison of the service life in mortars with various porosities of 0.25, 0.29, and 0.35 exposed to Na_2SO_4 solutions.

Porosity of mortar	Service-life (years)
0.25	340
0.29	290
0.35	240

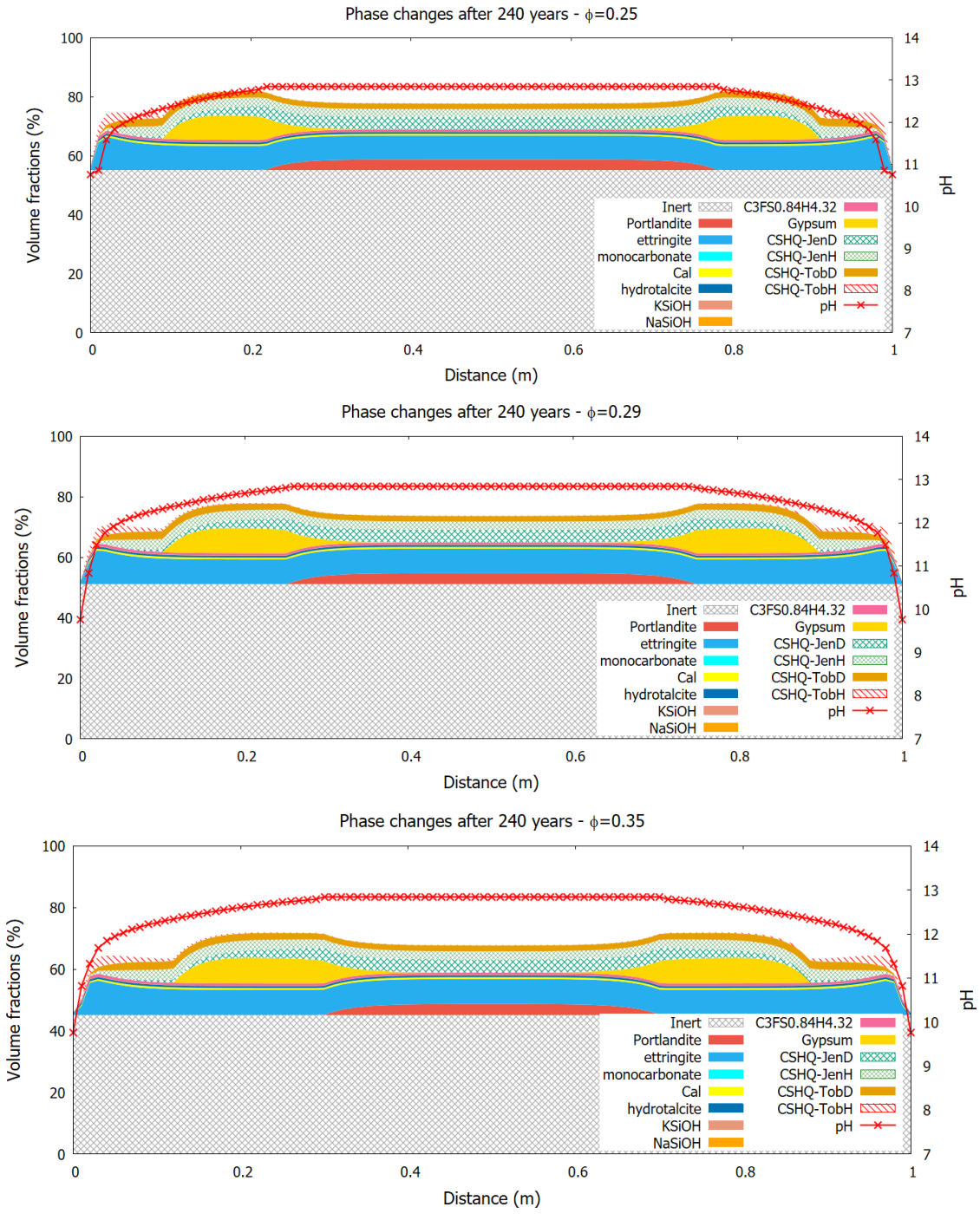

Figure 11: Comparison of the profile of the mineralogical phases in the mortar with various porosities of 0.25, 0.29, and 0.35 exposed to Na_2SO_4 solutions for 240 years.

Conclusions and summary

This report summarised the work that has been done in the WP2 of the SAFER2028 FN-CAMP project during 2024. In the first task, the assessment tool simulating the ASR in concrete was explored in sensitivity analyses, assessing the impact of temperature and relative humidity on ASR expansion. It was found that temperature influences the expansion rates, i.e., a higher temperature leads to faster kinetics. An impact of temperature on final expansion was observed, i.e., a higher temperature leads to a higher final expansion. This was because the final expansion was calculated based on incremental deformation as a function of time, where faster incremental kinetics at higher temperatures were considered. However, this was not consistent with the literature, where a limited or negative impact of temperature on final expansion was reported. Thus, it was recommended to use normalized expansion instead of final expansion in the current model. The impact of RH on ASR expansion was also investigated, and a threshold for initiating ASR was found. According to the sensitivity analysis results, no expansion was observed at RH of 50%, slight expansion started when RH increased up to 70%, and significant expansion was observed when RH was above 90%. The findings confirmed the results from earlier published studies and suggested that employing a low relative humidity (RH) can help reduce ASR expansion. In the following year, sensitivity analyses on the impact of loading states on expansion will be performed.

In the second task, the performance of mortars exposed to Na_2SO_4 solution and Na_2SO_4 + NaOH solution were investigated. In the former simulation case, it was observed that cementitious phase changes started from the replacement of monocarbonate by ettringite, followed by the dissolution of CH, decalcification of C-S-H, and precipitation of gypsum in addition to ettringite. Gypsum was observed to dissolve when pH decreases below 12.5. It was after 290 years that the calculation was stopped and all cementitious materials at the very border were consumed. The durability of mortars was significantly improved when being exposed to Na_2SO_4 + NaOH solution, where a pH of 13 was maintained by adding NaOH to prevent leaching. The formation of gypsum was not observed during exposure, as the pH of the pore solution in the mortar remained at 13. After being exposed for 1000 years, the dissolution of CH reaches the depth of 0.25 m from the boundaries, and an obvious increase in porosity is only observed at the very border. The results indicate the importance of a high pH for keeping high durability performance in cement-based materials. Sensitivity analysis on the impact of porosity of mortars was performed, considering values of 0.25, 0.29, and 0.35. The predicted service life was 340, 290, and 240 years respectively. Thus the importance of low permeability and porosity for improving long-term durability safety was highlighted. In the next step, the performance of cementitious materials exposed to a more complicated scenario will be simulated and investigated, i.e., groundwater and seawater, which will provide us with a better understanding of concrete when exposed to a more aggressive aqueous environment.

References

[1] Yushan GU, “Assessment of alkali-silica reaction and aggressive aqueous attack in concrete 2023,” 2023.
[2] V. Saouma and L. Perotti, “Constitutive model for alkali-aggregate reactions,” *ACI Mater J*, vol. 103, no. 3, 2006, doi: 10.14359/15853.
[3] D. W. Hobbs, *Alkali-silica reaction in concrete*. Thomas Telford Publishing, 1988.
[4] F. Glasser, “Chemistry of the alkali-aggregate reaction,” in *The alkali-silica reaction in concrete*, CRC Press, 1991, pp. 30–53.
[5] J. Lindgård *et al.*, “The EU ‘PARTNER’ Project - European standard tests to prevent alkali reactions in aggregates: Final results and recommendations,” *Cem Concr Res*, vol. 40, no. 4, 2010, doi: 10.1016/j.cemconres.2009.09.004.
[6] C. Larive, “Apports combinés de l’expérimentation et de la modélisation à la compréhension de l’alcali-réaction et de ses effets mécaniques,” Ecole nationale des ponts et chaussees, 1997.
[7] S. Diamond, R. S. J. Barneyback, and L. J. Struble, “On the Physics and Chemistry of Alkali-Silica Reactions,” *5th Conference on Alkali-Aggregate Reaction in Concrete*, 1981.
[8] Y. Kawabata, K. Yamada, Y. Sagawa, and S. Ogawa, “Alkali-Wrapped Concrete Prism Test (AW-CPT) - New testing protocol toward a performance test against alkali-silica reaction-,” *Journal of Advanced Concrete Technology*, vol. 16, no. 9, 2018, doi: 10.3151/jact.16.441.
[9] R. N. Swamy, “The alkali-silica reaction in concrete,” 1992.
[10] S. Chatterji and P. Christensen, “Studies of alkali-silica reaction. Part 7. Modelling of expansion,” *Cem Concr Res*, vol. 20, no. 2, pp. 285–290, Mar. 1990, doi: 10.1016/0008-8846(90)90082-9.
[11] B. Fournier, R. Chevrier, M. de Grosbois, R. Lisella, K. J. Folliard, and J. H. Ideker, “The Accelerated Concrete Prism Test (60°C): Variability of Test Method and Proposed Expansion Limits,” in *12th International Conference on Alkali-Aggregate Reaction*, 2004.
[12] O. Olajide, M. Nokken, and L. Sanchez, “Review on the Role of Moisture and Temperature in Alkali-Silica Reaction (ASR),” in *Proceedings of the 16th International Conference on Alkali-Aggregate Reaction in Concrete (ICAAR)*, 2022, p. 31.
[13] H. Ólafsson, “The effect of relative humidity and temperature on alkali expansion of mortar bars,” in *Proc., 7th Int. Conf. on Alkali Aggregate Reaction in Concrete*, 1986, pp. 461–465.
[14] U. Ludwig, “Effects of environmental conditions on alkali-aggregate reaction and preventive measures,” in *Proc., 8th Int. Conf. on Alkali Aggregate Reaction in Concrete*, 1989, pp. 583–596.
[15] T. Kurihara and K. Katawaki, “Effects of moisture control and inhibition on alkali silica reaction,” in *Proc., 8th Int. Conf. on Alkali-Aggregate Reaction, Elsevier, Amsterdam, Netherlands*, 1989, pp. 629–634.
[16] J. Lindgård, Ö. Andiç-Çakir, I. Fernandes, T. F. Rønning, and M. D. A. Thomas, “Alkali-silica reactions (ASR): Literature review on parameters influencing laboratory performance testing,” 2012. doi: 10.1016/j.cemconres.2011.10.004.
[17] F.-J. Ulm, O. Coussy, L. Kefei, and C. Larive, “Thermo-Chemo-Mechanics of ASR Expansion in Concrete Structures,” *J Eng Mech*, vol. 126, no. 3, pp. 233–242, Mar. 2000, doi: 10.1061/(ASCE)0733-9399(2000)126:3(233).
[18] J. Jabbour, A. Darquennes, L. Divet, R. Bennacer, J. M. Torrenti, and G. Nahas, “New experimental approach to accelerate the development of internal swelling reactions (ISR) in massive concrete structures,” *Constr Build Mater*, vol. 313, 2021, doi: 10.1016/j.conbuildmat.2021.125388.
[19] B. Capra and J. P. Bournazel, “Modeling of induced mechanical effects of alkali-aggregate reactions,” *Cem Concr Res*, vol. 28, no. 2, 1998, doi: 10.1016/S0008-8846(97)00261-5.
[20] A. B. Poole, “Introduction to alkali-aggregate reaction in concrete,” in *The alkali-silica reaction in concrete*, CRC Press, 1991, pp. 1–29.
[21] O. D. Olajide, M. R. Nokken, and L. F. M. Sanchez, “Evaluation of the induced mechanical deterioration of ASR-affected concrete under varied moisture and temperature conditions,” *Cem Concr Compos*, vol. 157, p. 105942, Mar. 2025, doi: 10.1016/j.cemconcomp.2025.105942.

[22] M. Lei, L. Peng, C. Shi, and S. Wang, “Experimental study on the damage mechanism of tunnel structure suffering from sulfate attack,” *Tunnelling and Underground Space Technology*, vol. 36, 2013, doi: 10.1016/j.tust.2013.01.007.
[23] Y. Wang and Y. Yao, “Researches on key engineering concrete durability and applications,” *China Building Materials, Beijing*, 2001.
[24] J. Marchand, I. Odler, and J. P. Skalny, *Sulfate Attack on Concrete*. CRC Press, 2001. doi: 10.4324/9780203301623.
[25] C. Ouyang, A. Nanni, and W. F. Chang, “Internal and external sources of sulfate ions in portland cement mortar: two types of chemical attack,” *Cem Concr Res*, vol. 18, no. 5, 1988, doi: 10.1016/0008-8846(88)90092-0.
[26] J. G. Wang, “Sulfate attack on hardened cement paste,” *Cem Concr Res*, vol. 24, no. 4, 1994, doi: 10.1016/0008-8846(94)90199-6.
[27] J. R. Clifton and J. M. Pommersheim, *Sulfate Attack of Cementitious Materials: Volumetric Relations and Expansions*, vol. NISTIR 5390. 1994.
[28] C. Yu, W. Sun, and K. Scrivener, “Mechanism of expansion of mortars immersed in sodium sulfate solutions,” *Cem Concr Res*, vol. 43, no. 1, 2013, doi: 10.1016/j.cemconres.2012.10.001.
[29] B. Tian and M. D. Cohen, “Does gypsum formation during sulfate attack on concrete lead to expansion?,” *Cem Concr Res*, vol. 30, no. 1, 2000, doi: 10.1016/S0008-8846(99)00211-2.
[30] T. Schmidt, B. Lothenbach, M. Romer, J. Neuenschwander, and K. Scrivener, “Physical and microstructural aspects of sulfate attack on ordinary and limestone blended Portland cements,” 2009. doi: 10.1016/j.cemconres.2009.08.005.
[31] M. Santhanam, M. D. Cohen, and J. Olek, “Mechanism of sulfate attack: A fresh look - Part 1; Summary of experimental results,” *Cem Concr Res*, vol. 32, no. 6, 2002, doi: 10.1016/S0008-8846(02)00724-X.
[32] E. F. Irassar, V. L. Bonavetti, and M. González, “Microstructural study of sulfate attack on ordinary and limestone Portland cements at ambient temperature,” *Cem Concr Res*, vol. 33, no. 1, 2003, doi: 10.1016/S0008-8846(02)00914-6.
[33] B. Lothenbach *et al.*, “Cemdata18: A chemical thermodynamic database for hydrated Portland cements and alkali-activated materials,” *Cem Concr Res*, vol. 115, 2019, doi: 10.1016/j.cemconres.2018.04.018.
[34] D. A. Kulik, “Improving the structural consistency of C-S-H solid solution thermodynamic models,” *Cem Concr Res*, vol. 41, no. 5, 2011, doi: 10.1016/j.cemconres.2011.01.012.
[35] D. A. Kulik *et al.*, “GEM-Selektor geochemical modeling package: Revised algorithm and GEMS3K numerical kernel for coupled simulation codes,” *Comput Geosci*, vol. 17, no. 1, 2013, doi: 10.1007/s10596-012-9310-6.
[36] J. Samper *et al.*, “Conceptual model formulation for a mechanistic based model implementing the initial SOTA knowledge (models and parameters) in existing numerical tools,” 2021.
[37] R. Ragoug, “Attaque sulfatique externe des matériaux cimentaires: Impact de différents facteurs âge, composition du liant, présence de chlorures,” Université Paris-Est, 2016.
[38] ACI, “Slag Cement in Concrete and Mortar ,” *American Concrete Institute (233R–03)*, p. 233, 2011.
[39] O. M. Abdulkareem, A. Ben Fraj, M. Bouasker, L. Khouchaf, and A. Khelidj, “Microstructural investigation of slag-blended UHPC: The effects of slag content and chemical/thermal activation,” *Constr Build Mater*, vol. 292, 2021, doi: 10.1016/j.conbuildmat.2021.123455.
[40] F. Sajedi, H. A. Razak, H. Bin Mahmud, and P. Shafigh, “Relationships between compressive strength of cement-slag mortars under air and water curing regimes,” *Constr Build Mater*, vol. 31, 2012, doi: 10.1016/j.conbuildmat.2011.12.056.
[41] D. Jóźwiak-Niedźwiedzka, M. Dąbrowski, K. Bogusz, and M. A. Glinicki, “Influence of slag cement on the permeability of concrete for biological shielding structures,” *Energies (Basel)*, vol. 13, no. 17, 2020, doi: 10.3390/en13174582.
[42] A. Hadj Sadok and L. Courard, “Chloride diffusion and oxygen permeability of mortars with low active blast furnace slag,” *Constr Build Mater*, vol. 181, 2018, doi: 10.1016/j.conbuildmat.2018.06.036.

[43] B. S. Divsholi, T. Y. D. Lim, and S. Teng, “Durability Properties and Microstructure of Ground Granulated Blast Furnace Slag Cement Concrete,” *Int J Concr Struct Mater*, vol. 8, no. 2, 2014, doi: 10.1007/s40069-013-0063-y.

Certificate Of Completion

Envelope Id: 46A13E5B-41C3-4CBE-B367-C9A648C789D0
Status: Completed
Subject: Complete with Docusign: VTT_R_00725_24
Source Envelope:
Document Pages: 21
Signatures: 1
Certificate Pages: 1
Initials: 0
AutoNav: Enabled
EnvelopeId Stamping: Enabled
Time Zone: (UTC+02:00) Helsinki, Kyiv, Riga, Sofia, Tallinn, Vilnius

Envelope Originator:
Erja Schlesier
Tekniikantie 21, Espoo
., . P.O Box1000, FI-0204
Erja.Schlesier@vtt.fi
IP Address: 130.188.133.34

Record Tracking

Status: Original
17 March 2025 | 13:54
Holder: Erja Schlesier
Erja.Schlesier@vtt.fi
Location: DocuSign

Signer Events	Signature	Timestamp
Miguel Ferreira miguel.ferreira@vtt.fi Research Team Leader Security Level: Email, Account Authentication (None), Authentication	DocuSigned by: 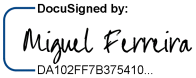 DA102FF7B375410... Signature Adoption: Pre-selected Style Using IP Address: 93.106.183.65	Sent: 17 March 2025 | 14:00 Viewed: 17 March 2025 | 19:42 Signed: 17 March 2025 | 19:43

Authentication Details
SMS Auth:
Transaction: 15d9c914-d87f-4f4c-916a-428417926728
Result: passed
Vendor ID: TeleSign
Type: SMSAuth
Performed: 17 March 2025 | 19:42
Phone: +358 40 1380546

Electronic Record and Signature Disclosure:
Not Offered via Docusign

In Person Signer Events	Signature	Timestamp

Editor Delivery Events	Status	Timestamp

Agent Delivery Events	Status	Timestamp

Intermediary Delivery Events	Status	Timestamp

Certified Delivery Events	Status	Timestamp

Carbon Copy Events	Status	Timestamp

Witness Events	Signature	Timestamp

Notary Events	Signature	Timestamp

Envelope Summary Events	Status	Timestamps
Envelope Sent	Hashed/Encrypted	17 March 2025 | 14:00
Certified Delivered	Security Checked	17 March 2025 | 19:42
Signing Complete	Security Checked	17 March 2025 | 19:43
Completed	Security Checked	17 March 2025 | 19:43

Payment Events	Status	Timestamps